A MODEL OF THE β - δ PHASE TRANSITION IN PBX9501

L. Smilowitz, B. F. Henson, B. W Asay, and P. M. Dickson

Los Alamos National Laboratory

Los Alamos, New Mexico 87545

In this paper we present second harmonic generation (SHG) experiments designed to confirm the mechanism and quantify the transformation kinetics of the β–δ solid state phase transition in octahydro-1,3,5,7-tetranitro-1,3,5,7-tetrazocine (HMX). We present a new kinetic model based on an extensive experimental study of the transition both from β to δ and from δ to β phases in PBX 9501. The mechanism for the transition is reversible nucleation and growth based on experimental observations of the phase transition. The model is therefore a two state kinetic model of the transition based on a rate law involving reversible components both first order in the β or δ mole fraction, simulating nucleation, and second order in both the β and δ mole fraction, simulating growth. We compare the measured SHG intensity as a function of time for a range of temperatures with predictions of the two state kinetic model. We perform a set of parameter optimization calculations based on agreement with the predictions of the model. Optimization does not significantly change the kinetic parameters that are thermodynamically constrained by the model, but there is a distribution of parameters necessary to reproduce the nucleation kinetics observed.

INTRODUCTION

Octahydro-1,3,5,7-tetranitro-1,3,5,7-tetrazocine (HMX) has three stable polymorphs and a fourth hydrate. The beta and delta forms are associated with the insensitive and sensitive phases of the material. This work studies the solid state phase transformation between these two phases. A rate law is derived based on a mechanism of nucleation and growth with a subset of the rate constants in the law constrained by a thermodynamic model of the activated states involved. In this paper, we describe the results of second harmonic generation (SHG) experiments conducted to test the validity of the model as a description of the phase transition and to determine the remaining unconstrained degrees of freedom in the rate constants. Experiments were conducted on ensembles of free HMX crystals and a composite material, PBX 9501, composed of HMX crystals embedded in a visco-elastic polymer matrix.

We have previously reported[1] SHG measurements on samples of HMX crystals that demonstrate the utility of the technique as a probe of the integrated mole fraction of δ phase HMX. In this paper, we present a more extensive and quantitative survey of the temperature dependence of the rate of transformation using the integrated second harmonic signal. We present additional integrated SHG measurements aimed at understanding the mechanism of nucleation and the thermodynamic reversibility of the transition.

To further understand the relative roles of nucleation and growth in the transition and to quantify the kinetic model, we conduct an extensive parameter optimization by fitting

the integrated SHG data to model calculations of the appearance of the δ mole fraction as a function of time in several ways: first, by starting with the thermodynamic parameter set and letting the parameters vary to best fit the combined data sets, and then, by fitting the parameters to the individual data sets. Fitting to individual experiments results in a set of optimized parameters for each temperature at which measurements were made. We construct distributions from these sets and analyze the statistical description of the best single set of parameters for all temperatures. From this statistical description, important differences are observed for the parameter sets with which the nucleation and growth steps are modeled.

EXPERIMENTAL

The experimental work presented here is based on an application of SHG as a probe of the mole fraction of δ-HMX. We have demonstrated the utility of SHG in this application in a previous letter[1]. In the experiments reported here, we do not attempt to use absolute intensity measurements. Instead we normalize the SHG intensity to that from the fully converted sample and use the progress from zero to one as a measure of the transition from zero to 100% δ phase. We assume the mechanism of harmonic generation to be volumetric and fully coherent. We therefore interpret the SHG intensity as being proportional to the square of the delta mole fraction present in the sample.

A. Materials

For this study, we have used Holsten and UK HMX[2]. PBX 9501 is composed of a bimodal distribution of HMX crystals (~120 and 30 μm diameter) bonded with Estane and the eutectic mixture of bis(2,2-dinitropropyl)acetal and bis(2,2-dinitropropyl)formal. PBX 9501 samples are obtained by pressing molding powder made from 95% Holsten HMX with 2.5% estane and 2.5% of the plasticizer mixture by weight. HMX crystals used in the SHG imaging work were both Holsten HMX and UK HMX used as obtained with no further purifications.

B. Heat treatment

The experiments were conducted in a copper oven with optical access to allow careful, uniform heating of the samples. Samples consisted of either small pieces of PBX 9501 (4 x 4 x 1 mm) placed between sapphire windows or loose crystals of HMX affixed to the windows with optical adhesive. Several thermocouples are placed on the sample and oven to monitor and control the sample temperature. We have found that for heating rates of 0.08 K/s or slower, radial gradients across the samples of less than 0.5 K can be maintained. Typical heating profiles are a 0.08 K/s ramp to a temperature at which the phase transition can occur. The sample is then held at that temperature for thousands of seconds to allow the transition to proceed. Cooling is done at approximately 0.05 K/s to room temperature, or to some intermediate temperature below the delta phase stability temperature to allow the β-δ reversion to occur.

C. SHG kinetics

The total second harmonic light signal generated by the sample is monitored by a photomultiplier tube measuring the reflected SHG from the back of the sample. A small percentage of the laser intensity is split off and monitored to normalize out fluctuations in the laser intensity. The PMT signal is collected in a boxcar integrator and integrated with a 10 sec time constant. The integrated signal is normalized against the square of the laser intensity and recorded as a function of time during the heating and cooling of the sample.

D. Modeling

We interpret the measured kinetics as a function of temperature in terms of a reversible nucleation and growth mechanism. This gives us a model with 16 parameters that control the kinetics of the phase transition. We use several different approaches to fitting these parameters. We start with thermodynamically defined parameters and either individually optimize the parameters to each of the data sets taken over the range of temperatures, or define a global set of parameters optimized to all of the data sets simultaneously. The optimization routine used was a multidimensional direction set method, implemented with a modified Powell's routine[3]. This technique chooses a direction and finds the function minimum, then selects another direction and finds a new minimum, continuing until the global minimum is reached.

RESULTS

A. OBSERVATIONS

We have performed imaging experiments based on nonlinear light scattering that show that the transition proceeds through a nucleation and growth mechanism which is thermally activated and exhibits a sigmoidal dependence on the changing mole fraction of β to δ, indicative of a second order kinetic rate law. The phase transition is reversible when the temperature is subsequently reduced below the stability temperature of the δ phase and exhibits a first order dependence of the mole fraction of δ to β with time.

A summation of data for the phase transition in samples of an HMX plastic bonded explosive PBX 9501 obtained in this laboratory is presented in Fig. 1. [1,4,5] The data are plotted as the time to effect half the transition as a function of the inverse of the temperature. The square data points are δ–β reversion experiments and the circles are β–δ conversion. The triangle point is the observed temperature and time for the transition under laser heating reported in Ref [1]. The inverted triangle is a point not directly reported previously. Observations of shear induced ignition in gas gun experiments in our laboratory revealed interesting endothermic features[5]. Subsequent experiments under similar conditions involving pulsed laser illumination and imaging of generated second harmonic light revealed spatially local regions of high harmonic scattering efficiency that we have assigned to regions of δ-HMX. The point is plotted as the transition time and temperature determined from the endothermic features in Ref. [5]. We caution that a direct assignment of the phase as δ or α is not yet possible. Our assignment is consistent with all other observations of the transition upon heating, however. Experiments on the phase transition

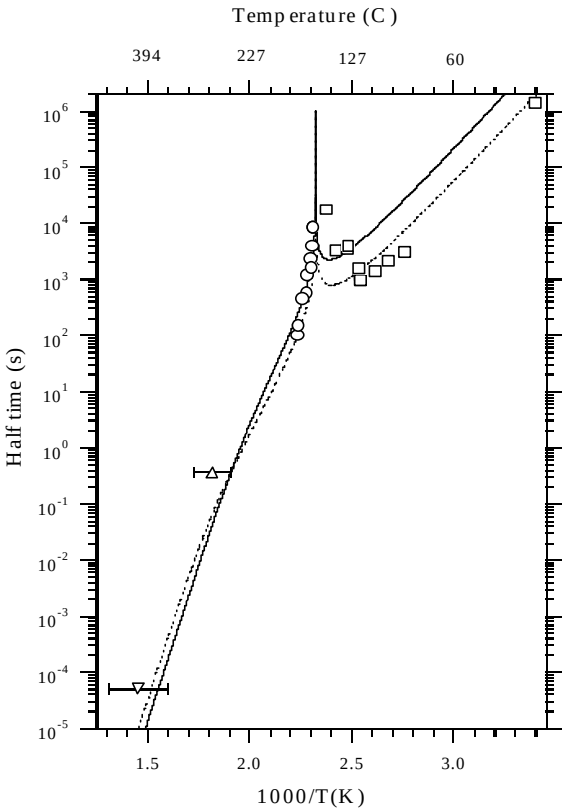

Figure 1: Compilation of data from kinetic measurements of the β-δ phase transition in PBX 9501.

under these conditions are ongoing.

The plot of ln(t) vs $1/T$ in Fig. 1 is the traditional Arrhenius plot. Linear regimes on such a plot are typically taken to denote regions dominated by a single Arrhenius rate constant with the slope determined by the activation energy. Given this traditional interpretation, the important features of the data are therefore (1) the observed kinetic slowing ($t \rightarrow \infty$) as the thermodynamic driving force goes to zero at the equilibrium transition temperature, (2) the activation enthalpy determined from the slope of the reversion rate at temperatures below the transition temperature, ≈ 69.4 kJ/mole, and (3) the change in slope at temperatures above the melting point of HMX represented by the line connecting the laser and shear induced transition times. The solid lines are calculations of the transition half time to be described below.

B. Modelling the Rate Law

The rate law is a differential equation intended to represent the key steps in the phase transformation. The four component processes, along with each labeled rate constant, are represented schematically, as follows

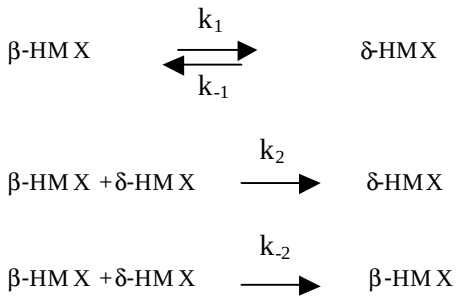

The first equilibrium step represents the nucleation kinetics from either β or δ phases. Step 2(a) and 2(b) represent the growth of the new, stable phase in either direction. The differential equation describing steps 1 and 2, written in terms of the δ and β mass fractions, is

$$\frac{\partial[\delta]}{\partial t} = k_1[\beta] + k_2[\beta][\delta] - k_{-1}[\delta] - k_{-2}[\beta][\delta] \tag{1}$$

In Eq. (1) the general features of the transition are captured as follows. The first order terms simulate the nucleation mechanism in the system, providing seed domains of the stable phase proportional to the fraction of the metastable phase. The second order terms in both β and δ simulate growth proportional to the growing interfacial area between domains as the new phase increases in size. This treatment is general to both phase transitions and diffusion limited chemical reactions in the solid state[6]. We divide Eq. (1) by the squared density of the β phase, β_o in order to obtain the mole fraction dependence

$$\frac{\partial x}{\partial t} = k_1 + (\beta_o(k_2 - k_{-2}) - (k_1 + k_{-1}))x + \beta_o(k_{-2} - k_2)x^2 \tag{2}$$

where $x = \delta/\beta_o$ is the mole fraction of the δ phase present in the sample. The first order rate constants k_1 and k_{-1} are in units of s^{-1} and the second order constants, k_2 and k_{-2}, are in units of $1/(s\beta_o)$, reflecting the second order kinetic dependence on concentration. Equation (2) thus represents a normalized scaling of the transition from 0 to 1 in the δ phase fraction. The magnitudes of the second order rate constants depend on the choice of units for the initial β phase concentration, β_o. We use β_o = 0.0063 mole/cm^3 for HMX in this paper, corresponding to the density of β-HMX.

C. Integrated Rate Equations

The integration of the rate law, Eq. (2), leads to a time dependent mole fraction that is a complex function of the time. The

requirement of real valued solutions and the application of appropriate boundary conditions allows the calculation of the equilibrium transition temperature dividing the regions of stability of the two phases. Integration with boundary conditions ranging from x = 0 to 1 leads to a real valued solution for temperatures greater than the stability temperature, representing the conversion of β to δ. Integration from x = 1 to 0 leads to a real valued solution for temperatures below the stability temperature, representing the reversion of δ to β. The integrated rate law in the mole fraction as a function of time is given by

$$x(t) = \frac{1}{2\beta_o(k_{-2} - k_2)}((k_{-1} + k_1) + \beta_o(k_{-2} - k_2) - \sqrt{B}\,\mathrm{Tan}(\mathrm{Arctan}(\frac{(k_{-1} + k_1) \pm \beta_o(k_{-2} - k_2)}{\sqrt{B}}) - \frac{1}{2}t\sqrt{B})) \quad (3)$$

where the positive signed numerator in the Arctan function denotes conversion from β to δ and the negative signed numerator reversion from δ to β. The constant B is the collection of rate constants

$$B = -k_{-1}^2 - 2k_{-1}(k_1 + \beta_o(k_{-2} - k_2)) - (k_1 + \beta_o(k_2 - k_{-2}))^2 \quad (4)$$

The temperature dependence of the rate law will be described below in the context of the rate constants. Here we solve for the transition time at some value of x, $t(x)$. We choose the inflection in the sigmoidal function, Eq. (3), which occurs at x = 0.5, as an extent of conversion for comparison at different temperatures. Eq. (2) solved for t with x = 0.5 is given by

$$t = \frac{2(A\mathrm{rctan}(\frac{((k_1 + k_{-1}) \pm \beta_o(k_{-2} - k_2))}{\sqrt{B}} - A\mathrm{rctan}(\frac{(k_1 + k_{-1})}{\sqrt{B}}))}{\sqrt{B}} \quad (5)$$

where the positive signed numerator in the Arctan function denotes conversion from β to δ and the negative signed numerator denotes reversion from δ to β.

D. Kinetics

We have measured the δ phase mole fraction change as a function of time in isothermal experiments over a temperature range from 362.6 to 447.0 K in continuous measurements and on samples cooled to ambient temperature, ~300 K, with periodic measurements over days. This model gives the delta volume fraction as a function of 16 parameters. Figure 1 shows the ability of the parameters defined thermodynamically to predict the kinetics of the phase transition as a function of temperature. The points are the measured half times for transition as a function of temperature in each of the experiments, and the dashed line is a calculation of the transition half time using Eq. (5). The halftimes are measured relative to the time at which the sample reaches 430 K. The predicted stability temperature separating β and δ HMX is 430.6 K. No conversion is thus expected at temperatures below this. The time between achieving 430.6 K and the temperature of the experiment thus introduces some uncertainty in the temperature of the transition but is expected to have a small effect on half times. For long times and low temperatures, this effect is certainly negligible, though it is one of the factors that limits the high temperature range of our isothermal experiments. As the temperature increases above 430.6 K, the conversion occurs faster. Our experiments are limited by how rapidly we can bring the entire sample to its set point temperature. For higher temperatures and therefore shorter conversion

times, our measured half times will be convolved with the temperature ramp times. For this reason, we have limited our temperature range to below 448 K. The low temperature side of the curve is limited by the exponential slowing of the transition time as we approach the equilibrium temperature.

In Fig. 2, both the half times and the conversion curves are shown with different fitting schemes. The left hand panels show the half time points and the fits from different parameter sets. The right hand panels show the full conversion experiments for a representative subset of four of the points from the half time plots. The points are the SHG data demonstrating the increase in SHG as the sample transforms from the beta to the delta. The solid lines through the points are the calculated delta mole fraction using Eq. (1) and a particular parameter set. The left panels show how a particular fitting scheme captures the dependence of the half time on temperature while the right panels show how well it can capture the details of the conversion process at each temperature.

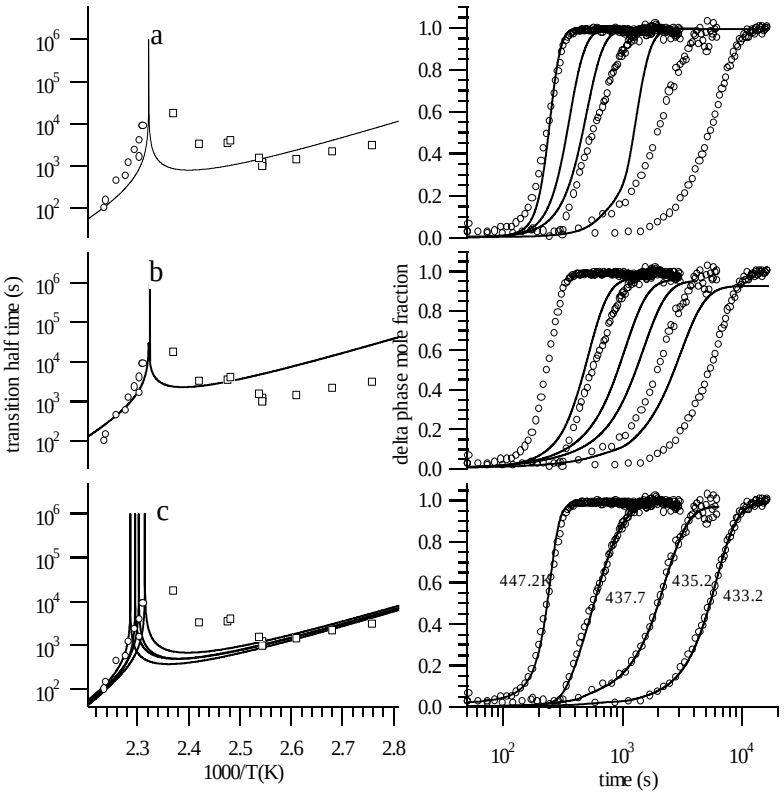

Figure 2: Left hand panels are a compilation of the measured halftime of the transition from each of the measurements. The data are plotted as the time to half conversion as a function of 1000/T(K), where T(K) is the isothermal temperature. Both β-δ conversion (circles) and δ-β reversion (squares) data are shown. Right hand panels are integrated SHG experiments at four representative temperatures.

Although we see on the half time plot of Fig. 2(a), that the thermodynamic parameters from the previous paper describe the half time for the phase transition well, we can see on the kinetic plot shown at the right hand side of Fig. 2(a), that the individual phase transition kinetics are not all well described by this single set of parameters, particularly as the temperature approaches the phase stability temperature for the beta phase. Starting with these thermodynamic parameters as our initial guess, we have allowed the parameters to vary and have optimized the set both individually to the kinetic data at each temperature and to the kinetic data of all the experiments simultaneously. For the simultaneous optimization, we fixed the difference between the forward and reverse parameters to the enthalpy, entropy, and volume differences of the beta and delta phases which have been reported in the

literature. We then let the linked forward and reverse parameters vary to minimize the RMS difference between the combined data sets and the model predictions. As given in Table I, the resulting parameter set is very close to the initial thermodynamic guess. Fig. 2(b) shows how this single optimized set of parameters can fit both the half times and the kinetic behavior of each data set. It fits the half times quite well over the full range of temperatures. However, it misses the kinetic behavior for the lower temperature data sets. If we individually optimize the parameters for each temperature, we can model the kinetic behavior of each set much better with a range of parameters. Figure 2(c) shows the fit to four individual data sets where the parameters have been optimized for each experiment. The left frame of Fig. 2(c) shows the thermodynamic predictions for half times for each of the optimized data sets used in the kinetic prediction. Each individual data set predicts a slightly different equilibrium temperature with the equilibium temperature increasing with the isothermal temperature of the experiment.

We have also measured the kinetics of the δ-β reversion transition. We have found that we can control the reversion to the β phase by controlling the cooling rate and temperature of the material. Differential scanning calorimetry (DSC) was performed on the samples to confirm full reversion to the beta phase as well. It showed the integrated endotherm had the same total energy as for a pristine sample, whereas a sample which was cooled quickly to trap it in the delta phase showed no endotherm. The importance of this observed dependence on rate and temperature in reversion to understanding the literature on reversion in this system will be discussed below [7,8]. Also, we have consistently observed an apparently first order single

	Thermodynamic (J/mole)	Simultaneous (J/mole)	Average (J/mole)	Percent Standard deviation
H_1	207691.0	206111.0	200177.0	0.3
H_{-1}	197891.0	196311.0	190857.0	1.0
H_2	79700.0	80346.3	78001.4	0.0025
H_{-2}	69900.0	70546.3	61902.5	0.04
S_1	144.438	149.547	136.891	2.0
S_{-1}	121.678	126.787	116.107	4.0
S_2	149.850	138.998	141.943	0.015
S_{-2}	127.090	116.238	104.939	0.15

Table I: Table of parameters for the rate constants described by Eq. (4) using a quadratic SHG dependence on delta fraction. Column 1 is the set of thermodynamically defined parameters. Column 2 is the set of parameters determined by simultaneously optimizing the model to all the data sets. Column 3 is the average of the parameter sets obtained by individually optimizing the parameters to each data set. Column 4 is the standard deviation for the average parameter set.

exponential dependence of the δ mole fraction with time in these reversion measurements. The model, however, produces the same second order sigmoidal curves in reversion as are observed in the β-δ conversion. This discrepancy is the major weakness in the current model and will also be discussed below.

We performed a number of experiments on samples of PBX 9501 where the transition is followed through two cycles by repeated heating and cooling. Considerable crystal damage, in the form of cracking on the few hundred nanometer length scale, accompanies the transition, and it is important to understand the ramifications of this irreversible component of the transition both on the SHG observable and measured kinetic parameters. The transition exhibits good reversibility with respect to the second harmonic intensity.

DISCUSSION

A. Standard deviation of thermodynamic parameters

As listed in Table I, the experimentally determined parameters are in fair agreement with the thermodynamically based parameters. The final column in Table I gives the standard deviation of the parameters optimized to the individual data sets for best kinetic fits of each. In particular, the parameters for k_2 and k_{-2}, describing the growth step have relatively small standard deviations, with mean values in agreement with the values for the enthalpy and entropy of fusion for HMX[910]. This result supports the model of the transition presented. Larger standard deviations, on the order of a few percent, are found in the nucleation parameters. This sample variability is under investigation in our laboratory and will be discussed in future work. A dependence on a distribution of defect states would be consistent with the observation of a range of nucleation energies.

B. Reversability of transitions

The thermodynamically stable phase of HMX at standard temperature and pressure is the β phase[7]. However, rapid cooling and control of temperature may be used to kinetically trap HMX in the metastable δ phase at temperatures below the transition temperature. This dependence on temperature history has been noted in previous work[11], and explains at least some of the wide range of previously reported stability times for the metastable δ phase upon cooling to room temperature[8]. The reversibility of the transition and the ability to kinetically freeze in a metastable phase give us a tool to separate out effects of mechanical changes from effects of phase changes. Such kinetic trapping, where the reduction in temperature reduces the rate of reversion to the point where no transformation takes place on the time scale of an experiment, is fully consistent with the thermally activated rate law and mechanism. The model presented here thus provides a quantitative mechanism to understand at least the temperature dependence of phase growth and its effect on metastability. Finally, as mentioned in Sec. III.B., although we have assumed a fully symmetric, reversible nucleation and growth model in order to take into account our observation of the reversibility of the phase transition, we are currently unable to reproduce the apparent first order behavior of the reversion to beta. The model does seem to approximately reproduce the temperature dependence of the reversion rate, however, as illustrated in the half life data and calculations of Fig. 1. It thus seems that the rate constants are at least approximately correct but some problem with order or stoichiometry exists in the present rate law. Another possible problem would be the neglect of the α phase in this law. We have observed α-HMX in some cooling experiments and plan to expand

the law to a three state system. This will be the topic of future work.

By cycling a sample through the β–δ conversion, reversion back to β phase, and then a second conversion to δ phase, we can test the effects of irreversible work done during the initial conversion process on the phase transition kinetics. Because the change in surface area generated by cracking of the sample during the phase change is irreversible upon cooling the sample while the SHG signal is reversible, this confirms the source of the SHG as a volumetric phase transition and shows that the contribution to the SHG from the surface area generated by cracking does not have a significant contribution to the SHG signal. Also, the kinetics of the second conversion process and the integrated area of the endotherm closely match the original onset behavior implying that the nucleation and growth rates are insensitive to the degree of cracking of the sample as well.

C. Nucleation mechanism

Additional questions remain about the mechanism(s) of nucleation in this system. Nucleation has been qualitatively shown to be a significant component of the synthesis of and transformation between HMX polymorphs[7]. We have observed significant differences in the behavior of PBX formulations and bare HMX crystals. The two most significant differences include the variable nucleation time in ensembles of HMX crystals compared to the uniform nucleation in PBX9501 discussed in Sec. IIIA. and the fact that we have not been able to induce reversion in HMX crystals by temperature control similar to that described in Sec. IV.C. We do not currently have a thermodynamic or defect state identified as the nucleation transition state. Phenomenologically, the observation that nucleation in crystalline HMX occurs at a small number of discrete sites, and that the addition of the binder in the PBX9501 has a large effect on the spatial mechanism of the transition, is presumably a reflection of the nucleation mechanism. We believe this is due to the solvation effect of the nitroplasticizer in the binder on the HMX crystals. This would be qualitatively consistent with observations by Cady[7] where interconversion and synthesis of HMX polymorphs was observed to be strongly affected by the solvent environment. Further work is under way to establish a correlation between solvent effects of different binder formulations and phase transition kinetics in order to establish a quantitative mechanism of nucleation.

D. Pressure dependence

The significant volume changes between the phases of HMX will likely make the phase transition kinetics dependent on pressure as well as temperature. We are investigating the traditional PΔV term in the free energy of the activated state as an adequate modeling parameter to account for the pressure dependence. Given the equilibrium volume changes, we expect to need pressures on the order of 10^8 Pa in order to observably affect the kinetics. However, this is on the order of the yield strength and will not be supported in the crystal. We therefore don't expect to see the kinetics modified by the internal stress state of the crystal induced during the phase change. We have begun work to directly verify the quasistatic pressure dependence of the kinetics in this system under both hydrostatic and non-hydrostatic conditions in a diamond anvil cell.

CONCLUSIONS

We conclude that the β to δ phase transition in PBX 9501 proceeds through reversible nucleation and growth of the delta phase. It is a thermodynamically first order phase transition whose kinetics are governed by a mixed second order reaction mechanism. Using the experimental observation of the transition state being the melt state, we are

able to determine the governing rates based almost entirely on independently obtained entropies and energies[7]. These rate equations provide an excellent prediction for transition times as a function of temperature over a broad range of times and temperatures. The model additionally is able to predict the detailed kinetic behavior of the phase transition at each temperature. Observation of reverse delta to beta phase transitions upon cooling to temperatures below the delta phase stability point led us to use a fully reversible nucleation and growth model. Although the thermodynamics predicted by this model approximately capture the reversion process, the details of the behavior are not captured. This work, although it represents significant progress in our understanding of HMX phase transitions, represents a working model which we will continue to refine. Further work is underway to understand the detailed mechanism for the reverse phase transitions, including the possible impact of a third phase appearing during reversion. All work to date has been performed at atmospheric pressures. Future work will address the question of how pressure will impact the dynamics of the transition through the volume change between the phases.

This is a comprehensive phase transition model for PBX9501. HMX crystals display a wider range of behaviors because PBX9501 averages out crystal size dependence and short circuits nucleation differences of individual crystals with the nitroplasticizer - crystal interaction. Another lesson of this work is that in order to determine the mechanism for the phase transition, it was necessary to look over a wide range of temperatures. This is demonstrated in Fig. 1 which spans 400C, and shows a complicated behavior with 3 slope changes and an asymptote. Fitting the mechanism for the kinetics at a single temperature or narrow temperature range, as shown in figure 2, doesn't elucidate the full behavior.

ACKNOWLEDGEMENTS

We wish to acknowledge the support of the Laboratory Directed Research and Development Program of Los Alamos National Laboratory and the continued support of the Los Alamos National Laboratory High Explosives Sciences Program administered previously by Phillip Howe, and presently by Deanne Idar.

REFERENCES

[1] B. F. Henson, B. W. Asay, R. K. Sander, S. F. Son, J. M. Robinson, and P. M. Dickson, Physical Review Letters **82**, 1213 (1999).

[2] Holsten HMX is synthesized in the US to a specification of less than 0.5% RDX (hexahydro-1,3,5-trinitro-1,3,5-trizocine) impurities. HMX synthesized in the UK typically exhibits a higher purity (<0.1%) with respect to RDX.

[3] W. H. Press, *Numerical Recipes in C: the art of scientific computing*. (Cambridge University Press, New York, 1988).

[4] B. F. Henson, L. B. Smilowitz, B. W. Asay, and P. M. Dickson, J. Chem. Phys., (2002).

[5] B. F. Henson, B. W. Asay, P. M. Dickson, C. Fugard, and D. J. Funk, presented at the Eleventh International Symposium on Detonation, Snowmass, CO, 1998 (unpublished).

[6] *Comprehensive Chemical Kinetics, Vol. II: The Theory of Kinetics*, edited by C. H. Bamford and C. F. H. Tipper (Elsevier, New York, 1969), Vol. vol. II.

[7] H. H. Cady, A. C. Larson, and D. T. Kromer, Acta Cryst. Sect. B **16**, 617 (1963).

[8] M. Herrmann, W. Engel, and N. Eisenreich, Zeitschrift Fur Kristallographie **204**(pt.1), 121 (1993).

[9] Y. Y. Maksimov, Zhurnal Fizicheskoi Khimii **66** (2), 540 (1992).

[10] The entropy can be calculated from $\Delta H=T\Delta S$ with and HMX melting point of 550K

[11] T. B. Brill and R. J. Karpowicz, Journal of Physical Chemistry **86** (21), 4260 (1982).